

Reactive Gas Magnetron Sputtering of Lithium Hydride and Lithium Fluoride Thin Films

G. B. Thompson and D. D. Allred

*Physics and Astronomy Department, Brigham Young University,
263 Fletcher Building Provo, Utah 84601*

Received February 4, 1997

We report the preparation and structural characterization of lithium hydride and lithium fluoride thin films. These materials, due to their low absorption in the soft x-ray range, may have a role as spacer layers in multilayer mirrors. Theoretical reflection calculations suggest that an epitaxial crystalline multilayer stack of a nitride and a lithium compound spacer layer could produce respectable reflectance for short soft x-ray wavelengths ($\lambda < 10$ nm). Lithium targets were magnetron sputtered in the presence of hydrogen or ammonia to prepare the LiH films and nitrogen trifluoride to prepare the LiF films. The films were deposited on room temperature Si (100) or MgO (100) substrates. A near IR-Visible-UV spectrometer indicated a drop in reflectance at ~ 250 nm for a 100-nm-thick LiH film. This corresponds to a 5-eV band gap (characteristic of LiH). UV fluorescence indicated characteristic LiH defect bands at 2.5, 3.5, and 4.4 eV. The UV fluorescence characterization also indicated a possible lithium oxide (Li_2O) contamination peak at 3.1 eV in some of our thin films. Film surface morphology, examined by scanning electron microscopy, appeared extremely rough. The roughness size varied with reactive gas pressure and the type of substrate surface. A LiH/MoN multilayer was constructed, but no significant d spacing peak was seen in a low angle $\text{CuK}\alpha$ XRD scan. It is believed that the roughness of the LiH film prevented smooth, uniform planar growth of the multilayer stack. Possible reasons of rough growth are briefly discussed. © 1997 Academic Press

1. INTRODUCTION

Lithium's optical properties in the soft x-ray region makes this element nearly transparent and therefore an ideal candidate as a spacer layer in multilayer mirrors. Unfortunately, this element is highly reactive making it unsuitable for multilayer applications. However, lithium compounds could still maintain similar transparent optical properties while being in a nonreactive state. This research was done to determine if lithium compound thin films could be reactively sputtered for such x-ray multilayer mirror applications. The compound structures reported in this paper are lithium hydride, LiH, and lithium fluoride, LiF.

2. BACKGROUND

To date, most spacer layers in x-ray optic multilayers are amorphous (1-4). Within most, if not all, of these multilayers, there is a region of interface mixing between the amorphous member and the high density member of the multilayer stack (5). This interface region is at least a few angstroms thick. While the effect on reflectance

of this mixing region is slight for d spacings (bilayer thickness) > 7 nm, it can dramatically lower the reflectance for d spacings lower than this value. As the wavelength of interest decreases, so does the need for the d spacing. Consequently, there has been a strong interest in producing improved small period multilayers.

Crystalline based materials have properties which would allow their structures to keep good contrast between interface layers in these lower d spacing regions. Epitaxial crystalline multilayers with sharp contrast between layer pairs for relatively small d spacings have been constructed for superconducting Josephson junction and advanced hardness coating studies (6, 7). Ideally, if the material is grown epitaxially, layer by layer, a bilayer thickness on the order of the crystalline lattice dimensions could be achieved.

It is well known that certain materials, under the proper growth conditions, can exhibit single crystal epitaxy (8). This type of growth can produce multilayer superlattices which have smooth surfaces over large areas, as well as possessing atomically abrupt interfaces. Yet the use of crystalline based multilayers in x-ray optics has lagged. This has resulted from the poor theoretical reflectance that most common, high quality, superlattice materials exhibit. For the superlattice materials with high optical contrast for x-ray reflectors, the fabrication of the multilayer can be difficult. These difficulties include lattice matching, surface tension, thermal chemical compatibility, and proper deposition temperatures. In short, for high-quality superlattice x-ray reflectors, both optical constants coupled with fabrication feasibility need to be considered.

We have identified B1 (rock salt) compounds, which have similar lattice constants (epitaxial growth), and good optical contrast needed to produce these types of superlattice x-ray reflectors. The crystalline structures proposed to develop these types of multilayers are LiH, LiF, and MoN. For example, a 500 layer pair epitaxial multilayer of LiH/MoN on a MgO (100) substrate at a d spacing of 1 nm for a wavelength of 2 nm would have a theoretical reflectance of 26% at near normal incidence compared to a comparable Mo/a-Si multilayer's 9% near normal reflectance. Magnetron sputtering has produced epitaxial multilayers with a d spacing of 0.96 nm (9). Therefore this deposition technique was used as a precursor to begin to investigate the construction of small d spacing, superlattice multilayers.

3. EXPERIMENTAL PREPARATION

The dc magnetron sputtering system employed was a custom built stainless steel chamber that housed two 10-cm-diameter targets. The chamber's base vacuum pressure was $\sim 5 \times 10^{-7}$ T and was produced by a cryopump and a mechanical roughing pump. The major contaminate of the system at this pressure was water vapor. The substrates are rotated ~ 25 cm above the target surface with planetary motion controlled by a computer driven stepping motor. The deposition area was defined by an 11-cm-diameter target with 25-cm-high cylindrical shields placed around each target. A Ferrin Scientific mass polarity analyzer (MPA) was attached to the chamber to allow the operator to monitor the individual gases in the system. Sputtering gases were flowed into the chamber via mass flow controllers and/or needle valves. Argon was used as the plasma gas source where hydrogen or ammonia was used as the hydride reactive

gas and nitrogen trifluoride was the fluoride reactive gas. Gibbs free energy calculations indicated that lithium in the presence of these gases would form the desired compounds on a room temperature substrate.

The lithium target consisted of a custom machined 10-cm-diameter, 0.6-cm-high, and 1.5-mm-wall-thickness aluminum dish in which lithium metal was compressed to completely fill the volume. The aluminum dish was used to fix the lithium into the desired target size. The cutting and pressing of the lithium into the aluminum dish was done quickly to minimize the oxidation of the metal. Once the lithium was pressed, the target was fixed to the sputtering gun in the magnetron sputtering chamber. A razor blade was used to scrape off surface oxide until the majority of the surface appeared to be metallic. Once the chamber was under a sufficient vacuum, the target was presputtered 10 to 20 min to remove any residual oxide. The indication of a "clean" lithium surface was a stable sputtering voltage. If the target had excessive oxide build up, the sputtering voltages would fluctuate. Sputtering voltages were 250 to 310 V for 80W. This voltage is much lower than voltages needed to sputter other active metals like titanium, tungsten, and molybdenum. Typical sputtering voltages for these refractory metals were in the 400 V range.

4. EXPERIMENTATION

Typical sputtering depositions involved evacuating the chamber to 5×10^{-7} to 1×10^{-6} T range starting with a 1-h bake-out. The cryopump was then throttled and the flow rate of Ar into the system was adjusted to the desired pressure ($1-2.5 \times 10^{-3}$ T). The flow rate of the reactive gases were adjusted to obtain the desired partial pressure which was in the mid- to high- 10^{-4} T range (during sputtering). Typical sputtering rates of lithium in the presence of the hydrogen and ammonia sources were 2.5 nm/min at 80 W. When nitrogen trifluoride was used, the sputtering rates decreased to 1.2 nm/min at 80 W (possible indication of fluoridation of the lithium target surface). For comparison, the typical deposition rate of molybdenum in the system was 1.8 nm/min for 100 W. MPA trend plots taken during sputtering showed the break down of the individual reactive gases into their respected atomic components. The MPA readouts also indicated, in some deposition runs, a background level of oxygen in the low- 10^{-7} T range. In other sputtering runs, oxygen could not be detected (below the 10^{-7} T scale). Oxygen could form Li_2O instead of the desired lithium compounds and its presence thereby would be a serious contamination problem.

The lithium compound films and lithium compound based multilayers were deposited onto either a Si (100) (with a native Si oxide surface layer) or a MgO (100) substrate. The substrates were used in an "as is" condition and were not intentionally heated or cooled during deposition [deposited at room temperature ($\sim 25^\circ\text{C}$)].

Typically LiH thin films were deposited to a thickness of 100 nm, while LiF thin films were deposited to a thickness of 50 nm. Thickness measurements were done by a Wykco visible light interferometer. The lower thicknesses of the LiF films was a result of deposition hindrances. The corrosive nature of the NF_3 gas caused the gas intake valves to degrade thereby reducing the ability to accurately control the flow of the gas. This action resulted in the fluoridation of the lithium target causing the

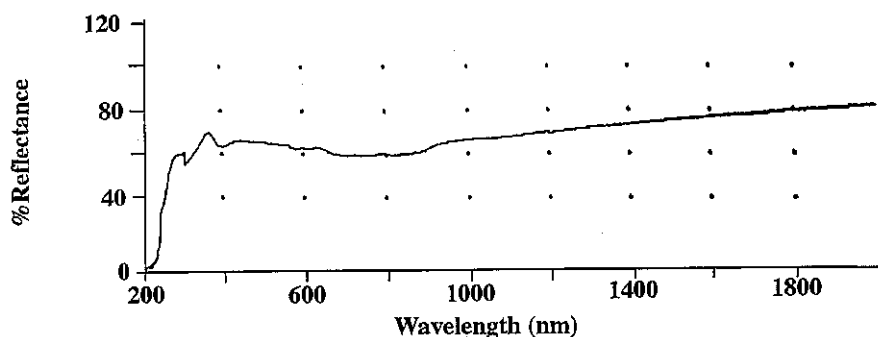


FIG. 1. A near IR-Visible-UV spectrometer reflection plot of a 100-nm-thick LiH film on Si (100). Note the drop in reflectance at ~ 250 nm. This corresponds to ~ 5 -eV band gap. The reactive sputtering gas was NH_3 at 0.75 mT.

sputtering voltages and currents to fluctuate. Monitoring the NF_3 gas pressure also proved difficult. The continual use of this gas degraded the MPA filament until it became useless.

5. CHARACTERIZATION

The transparency properties of the lithium compound films to traditional x-ray and to electron based characterization techniques made their analysis difficult. Below is a summary of the techniques and results which we found useful in studying the structures of the lithium compound films.

5.1. Visible-UV Techniques

A near IR-Visible-UV spectrometer was used to obtain the reflectance of the LiH films. Figure 1 shows a drop in reflectance below ~ 250 nm (~ 5 eV) for a 100-nm-thick LiH film on Si. This corresponds quite well with the 5.05-eV band gap of LiH (10, 11). At energies above the band gap, the reflectance is contributed to LiH, which is below 10%. The reflectance below the band gap is mostly contributed by the Si substrate (i.e., the film is transparent at these energies).

UV fluorescence of the hydride films could also indicate that the material was LiH by the presence of defect bands. Figure 2 is an emission mode plot with excitation near LiH's band gap for a 100-nm-thick LiH film on a Si (100) substrate. The high-intensity peaks at 250 nm (~ 5 eV), 500 nm (~ 2.5 eV), and 750 nm (~ 1.6 eV) are the orders of the excitation line and should be ignored. The peaks at 345 nm (3.5 eV) and 281 nm (4.4 eV), with an additional peak at 500 nm (2.5 eV), detected at a different excitation energy, are the emission bands due to defects in LiH (12). (The excitation energy line at 500 nm in Fig. 2 broadened and masked the 2.5-eV emission peak.) Figure 2 also indicates other emission peaks. The emission peak at 400 nm (3.1 eV) could correspond to oxide contamination since Ortman and Larsen have reported Li_2O spectra lines at ~ 563 nm (2.2 eV), 400 nm (3.1 eV), and ~ 318 nm (3.9 eV) (13), two of which were not seen on our emission plots. The broad peak

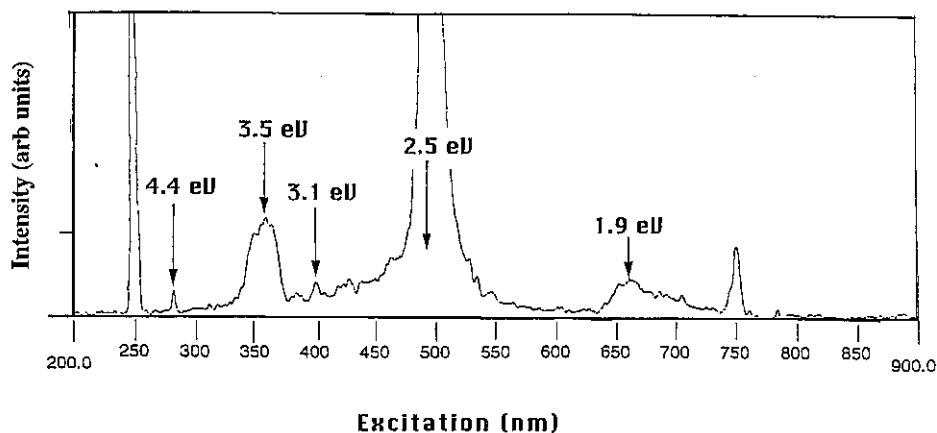


FIG. 2. A fluorescence emission plot with excitation at 250 nm, and integer orders thereof. The sample is a 100-nm-thick LiH film on Si (100). The reactive gas was NH_3 at 0.85 mT. Peaks at 2.5, 3.3, and 4.4 eV are characteristic defect bands of LiH. The peak at 3.1 eV is a possible indication of oxide contamination. The broad peak at 1.9 eV has not been identified.

at 653 nm (1.9 eV) has not yet been identified. Contamination from the oxygen could have been a result of residue oxide sputtered from the target surface, water vapor present in the chamber, a film-substrate interface oxide reaction (discussed later), and/or a minute air leak which was below the 10^{-7} T scale on our MPA. It should be noted that some LiH samples did not show the 400-nm emission peak. Lithium fluoride's high band gap (14.1 eV) prevented the use of this technique in its characterization. The limit of our fluorometer was ~ 6 eV.

5.2. Electron Diffraction Techniques

To further characterize the lithium compound films, electron backscatter diffraction (EBSP) was used. When the 100-nm-thick LiH film and the 50-nm-thick LiF film on Si (100) substrates were placed under the electron beam, a $\langle 100 \rangle$ diffraction pattern was seen. As the electron beam was moved to different areas on the film, the same pattern and orientation appeared. Since LiH and LiF deposited on Si should not have single crystal epitaxial growth, the diffraction image was concluded to be the diamond cubic structure of the silicon. The diamond cubic structure's diffraction pattern is very similar to that of the face centered cubic structure except that it has additional Kikuchi bands which originate from the center of the $\langle 100 \rangle$ zonal axis (14). The diffraction of these bands was not strong enough to be seen clearly beneath the LiH and LiF films. The ability to detect the silicon structure pattern through the thin lithium compound films demonstrates the electron transparency properties these materials have. This result indicates why lithium compound thin films appear so promising for short-wavelength optical applications.

Transmission electron microscopy (TEM) was also used to determine whether the lithium compound films would diffract the fcc structural pattern. LiH crystallites were deposited onto 3-mm-diameter commercial TEM carbon coated grids to a thickness



FIG. 3. A TEM image of LiH crystallites at 200 kV. The reactive gas was H_2 at ~ 0.5 mT. The inset shows the acquired diffraction pattern. The crystallites, in the imaging mode, appeared to be "moving" while under the electron beam, making their characterization difficult.

of 200 nm. The reactive gas was H_2 at ~ 0.5 mT. The TEM potential was 200 kV. Unfortunately, this technique was unable to produce a coherent ring diffraction pattern. In the image mode, the LiH crystallites appeared to be "moving." This "movement" was believed to be either a charging of the sample and/or the decomposition of the LiH into its atomic components by the heat generated from the focused electron beam on the sample. Figure 3 is a TEM image of the LiH crystallites.

5.3. Scanning Electron Microscopy

The final method of characterization of the LiH and LiF films was the study of its surface morphology by scanning electron microscopy (SEM). For imaging requirements, the thin films were sputtered with a 3- to 10-nm gold coating.

Figure 4 is a SEM image of a 100-nm-thick LiH film deposited onto a Si substrate. The reactive gas was NH_3 at 0.85 mT. The image shows that the film grew rough from the random ordering of the deposited LiH crystal structures. On higher magnification, the LiH crystallites appeared to be ~ 80 nm in diameter. Other LiH films deposited onto Si wafers at various reactive gas pressures (0.2 to 1 mT) and gases (NH_3 or H_2) showed similar rough surface morphology.

Figure 5 is a SEM image of a LiF film on Si. The film was deposited with NF_3 at 0.4 mT. The surface does not appear to be as rough as the LiH film but still maintains the inability to evenly and uniformly coat the substrate surface. The LiF crystallites appear oval like with the longest dimensions being 200–300 nm and the shortest dimension being 100 nm.

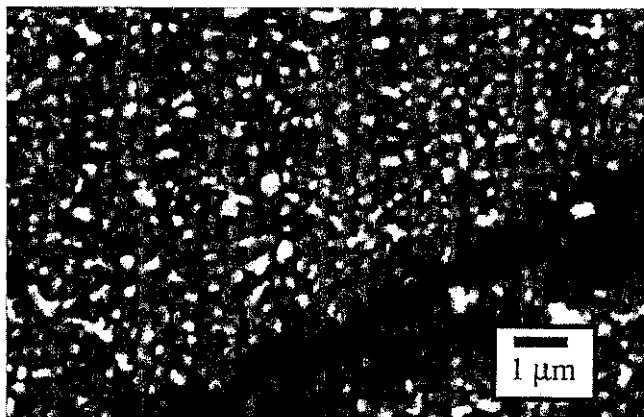


FIG. 4. A SEM image of a 100-nm-thick LiH film on Si (100), over coated with 10 nm gold for imaging requirements. The reactive gas was NH_3 at 0.85 mT. Note the rough surface morphology.

The LiH films were also deposited onto MgO (100) substrates to allow for the heteroepitaxy growth of the LiH rocksalt structure. Figure 6 is a SEM image of the LiH film deposited on MgO using NH_3 as the reactive gas at 0.85 mT. This image clearly shows much larger crystallites than those which were deposited onto the Si at the same reactive gas pressure (Fig. 4). The SEM image indicates three-dimensional island formation with much less lateral growth. This type of nucleation prevented long-range two-dimensional growth of the crystallites over the substrate surface.

When H_2 was used as the reactive gas source at 0.2 mT, the LiH crystallites on the MgO substrate showed more lateral growth but with a smaller crystallite size (see Fig. 7). This type surface morphology was very similar to that seen on the Si surfaces (Fig. 4).

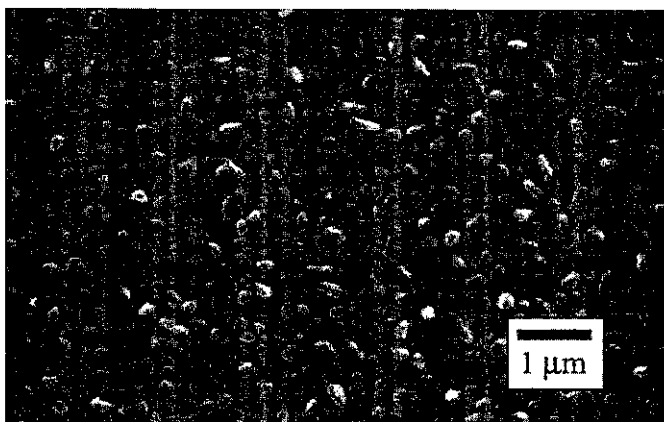


FIG. 5. A SEM image of a 50-nm-thick LiF film on Si (100), over coated with 10 nm gold for imaging requirements. The reactive gas was NF_3 at 0.4 mT. Note the rough surface morphology.

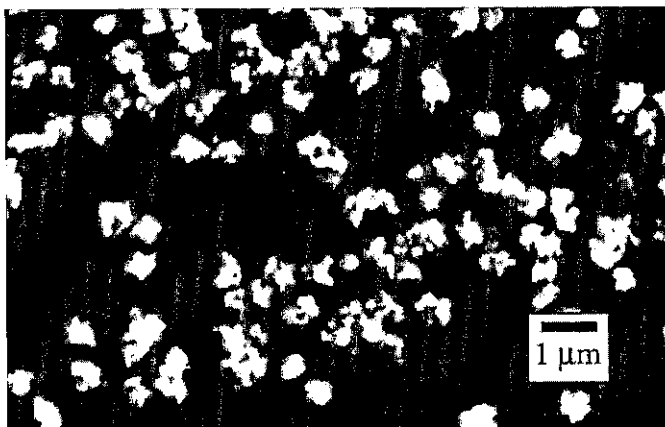


FIG. 6. A SEM image of a 100-nm-thick LiH film on MgO (100), over coated with 10 nm gold for imaging requirements. The reactive gas was NH_3 at 0.85 mT. The surface shows three-dimensional island formation with little lateral growth between crystals.

A construction of a LiH/MoN multilayer was attempted using ammonia's nitride and hydride components as the respected reactive gas for the Li and Mo sputtered elements. Two multilayers were made at two different reactive gas pressures. Each was deposited on a MgO (100) substrate with the parameters of a 7-nm bilayer thickness for 40 layer pairs. Figure 8 is the SEM image of the multilayer deposited with the reactive gas at 1 mT. As expected the surface was rough with no uniform planar growth. Figure 9 is a SEM image of a similar multilayer but deposited with a

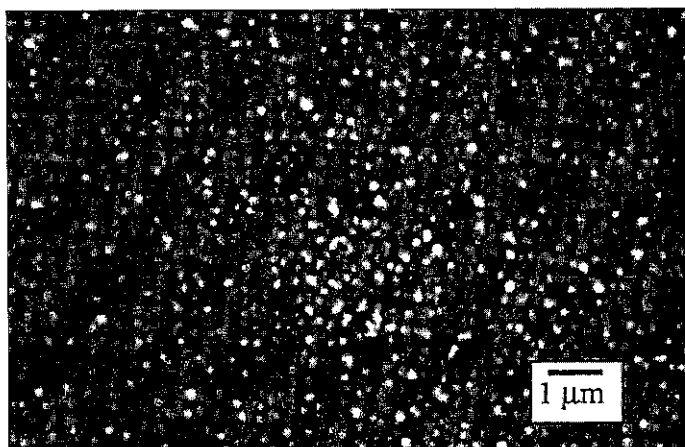


FIG. 7. A SEM image of a 100-nm-thick LiH film on MgO (100), over coated with 10 nm gold for imaging requirements. The reactive gas was H_2 at 0.2 mT. The lower molecular weight and reactive gas pressure produced LiH crystallites with more lateral growth and smaller sized crystallites when compared to Fig. 6.

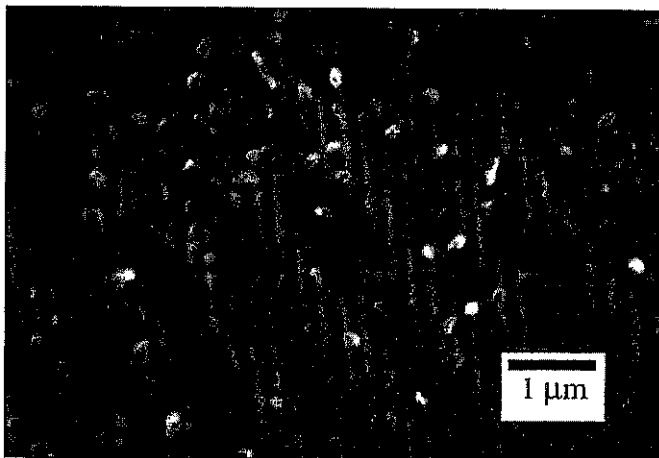


FIG. 8. A SEM image of a LiH/MoN multilayer on a MgO (100) substrate, over coated with 10 nm gold for imaging requirements. The deposition parameters are 40 layer pairs at a bilayer thickness of 7 nm. The reactive gas was NH_3 at 1 mT. As expected the surface was rough and no clear distinct bilayer spacing peak was seen in a low angle CuK_α XRD scan.

reactive gas at 0.3 mT. The surface is much smoother but in tensile stress. The tensile stress is evident by the planar cracks on the film surface. A low angle (0.5° to 8°) CuK_α x-ray diffraction (XRD) scan indicated no significant reflected peak for both multilayers, therefore no distinct d spacing. The relative smoothness of the multilayer films compared to LiH thin films at similar reactive gas pressures merits further investigation.

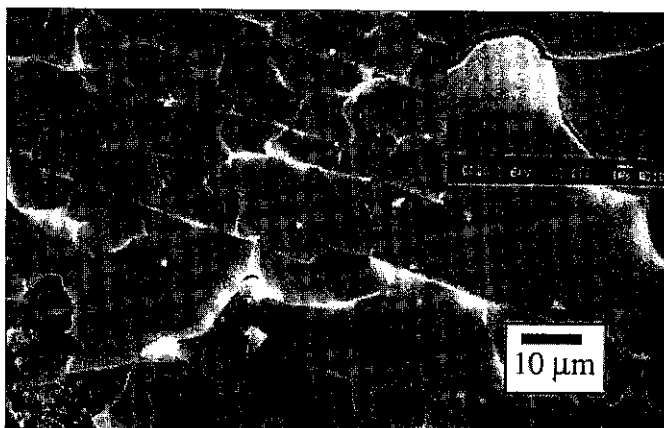


FIG. 9. A SEM image of a 280-nm-thick LiH/MoN multilayer on MgO (100), over coated with 10 nm gold for imaging requirements. Deposition parameters are 40 layer pairs at a bilayer spacing of 7 nm. The reactive gas was NH_3 at 0.3 mT. The film surface is smooth but in tensile stress (as evidenced by the surface cracks). A low-angle CuK_α XRD scan indicated no distinct bilayer spacing peak.

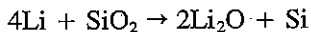
A LiF/MoN multilayer on Si was deposited with similar deposition parameters as listed above using NF_3 at 0.8 mT. Its surface, like the 1-mT LiH/MoN multilayer, was rough and indicated no significant reflected peak for a low-angle $\text{CuK}\alpha$ XRD scan.

6. DISCUSSION OF ROUGH GROWTH

Thornton's zonal model of surface morphology evolution may provide the beginnings for the possible reason on why the films grew rough (15). Thornton divided the surface morphology into various zones depending upon sputtering gas pressure and the ratio of substrate temperature to the melting point of the material. Even though Thornton studied thick sputtered metallic films (20–250 μm), his zonal model contains characteristics which were seen in the deposited lithium compound thin films. The sputtering pressures and substrate temperature would categorize the deposition of the films on the edge of zone 1 and zone T in Thornton's model. Characteristics of zone 1's oblique deposition and zone T's dense grain boundary arrays can be seen in Figs. 4, 5, 6, 7, and 8. But other characteristics from these zones, such as fibrous grain formation, are not seen on the SEM images.

In addition to Thornton's zonal model, the rough growth may be associated with mean free path. The substrates were held ~ 25 cm above and parallel to the target surface. At sputtering pressures of ~ 2 mT, the mean free path of a sputtered atom is ~ 2.5 cm, a factor of 10 smaller than the distance needed to travel to the substrate. This large difference in distance should result in numerous collisions of the sputtered atoms with the gaseous environment of the chamber. These collisions would reduce the energy of the atoms arriving at the substrate surface. Since LiH and LiF would have a low molecular weight relative to the other gases in the chamber (Ar and NH_3 or NF_3), such substantial differences in molecular weight could have also effected the collisions and energy kinetics of the arriving lithium compounds onto the substrate. Differences in surface roughness from the choice of reactive gases and their pressures can be seen in Figs. 6 and 7. The use of NH_3 showed large LiH crystallite formation with little lateral growth where H_2 at a lower reactive gas pressure indicated small crystallite formation with more lateral growth. Since each of these films were deposited on MgO substrates under similar Ar sputtering pressures, their surface formations could be concluded as differences in the type of collisions the arriving LiH had with the reactive gases in the chamber. The development of a LiH/MoN multilayer on a MgO substrate also indicated a significant difference in surface texture with reactive gas pressure as seen between Figs. 8 and 9.

A final possible reason for the rough growth could have been the oxide contamination within the film. Lithium oxide's antifructite cubic structure in which oxygen ions are in a fcc lattice with lithium ions in a simple cubic sublattice may have distorted the long range crystal growth of the fcc structure of the desired lithium compound. This oxide contamination, besides the possibility of it coming from the chamber environment, may have been a result of reactions of the film on the native Si oxide on the Si substrate surface. If pure lithium was deposited onto the SiO_2 surface, thermodynamics allows the possibility of Li to react at these surfaces.



Gibbs free energy calculations for such a reaction yielded a substantial negative ΔG (-267.8 kJ at 25°C). This type of reaction could account for the 3.1-eV (Li_2O) emission peak seen in the UV fluorescence characterization for the films deposited onto the Si substrates. Calculations for lithium on the MgO substrate interface yielded a slightly positive ΔG (6.8 kJ at 25°C), making such a reaction unfavorable.

7. CONCLUSION

The optical properties of lithium compound materials in the soft x-ray region makes them ideal candidates as multilayer spacer layers. Reactive gas magnetron sputtering has shown that these films can be deposited but with extreme surface roughing. We were able to see a possible correlation between roughness and type of reactive gas and pressure. This rough morphology may be a result of the mechanisms described in Thornton's zonal model, a small mean free path for the sputtered atoms, and/or oxide contamination. This type of growth will not allow for uniform planar interfaces to exist between thin film pairs. Other types of deposition methods, such as molecular beam epitaxy, have shown that rock salt structures can be deposited with a smoother surface morphology (16). Koster *et al.* have reported that electron beam evaporation of LiF will, in some circumstances, promote smooth growth of other fcc structures (17). Additionally, the electron gun deposition of MgO on LiF substrates produced more suitable surfaces (18). This indicates that other types of deposition techniques may be more appropriate for the construction of lithium compound multilayers.

This research supported that optical characterization of lithium compounds seems to be one of the few methods in which these structures can be studied. The transparency of the lithium compound films to electrons and to x-rays make their characterization difficult by these techniques.

ACKNOWLEDGMENTS

We thank David Field of TSL TexSEM Laboratories of Provo, UT, for his EBSP characterization and Pavel Brovkin of BYU for his help in SEM/UV fluorescence characterization. This work was funded by MOXTEK, Inc., of Orem, UT, and a grant from Brigham Young University's Office of Research and Creative Activities.

REFERENCES

1. U. Kleineberg *et al.*, *Appl. Opt.* **34**(28), 6506 (1995).
2. H. Kinoshita, K. Kurihara, and H. Takenaka, *Japan. J. Appl. Phys.* **30**(11B), 3048 (1991).
3. V. Dupuis *et al.*, *J. Appl. Phys.* **68**(10), 5146 (1990).
4. W. H. Wang, H. Y. Bai, and W. K. Wang, *J. Appl. Phys.* **74**(4), 2471 (1993).
5. D. L. Windt, R. Hull, and W. K. Waskiewicz, *J. Appl. Phys.* **71**(6), 2675 (1992).
6. K. Kawaguchi and S. Smith, *J. Appl. Phys.* **67**(2), 921 (1990).
7. D. W. Kim, Y. J. Park, J. G. Lee, and J. S. Chun, *Thin Solid Films* **165**, 149 (1988).
8. K. Takayanagi, K. Yagi, and G. Honjo, *Thin Solid Films* **48**, 137 (1978).
9. N. Hirashita and J. E. Greene, *J. Appl. Phys.* **70**(9), 4963 (1991).
10. G. I. Piliipenko, D. V. Oparin, and F. F. Gavrilov, *Solid State Commun.* **57**(11), 869 (1986).

11. A. V. Polienko, M.E. Tabachnik, S. O. Cholakh, A. A., and O'Connell-Bronin, *Phys. Stat. Sol.* **179**(411), 411 (1993).
12. M. Ikeya and T. Miki, *J. Luminescence* **12-13**, 333 (1976).
13. M. S. Ortman and E. M. Larsen, *J. Am. Ceramic Soc.* **66**(9), 645 (1983).
14. D. Field. [Private consultation, TSL TexSEM Laboratories, Provo, UT 84604]
15. M. Ohring, "*The Materials Science of Thin Films*," p. 223, Academic Press, San Diego, 1992.
16. D. A. Lapiano-Smith, E. A. Eklund, F. J. Himpsel, and L. J. Terminello, *Appl. Phys. Lett.* **59**(17), 2174 (1991).
17. S. Koster, N. Herres, M. Rey, and K. Reichelt, *J. Appl. Phys.* **59**(1), 278 (1986).
18. M. O. Aboelfotoh, *J. Appl. Phys.* **49**, 2270 (1978).